DOI: 10.13009/EUCASS2019-541

Testing 1kN Paraffin-Based Hybrid Rocket Engine

D. Cardillo, F. Battista*, M. Fragiacomo*, G. D. Di Martino**, G. Festa**, S. Mungiguerra** and R. Savino***
** CIRA (Italian Aerospace Research Centre), Via Maiorise, 81043 Capua (CE), Italy*
*** Università di Napoli Federico II, P.le Tecchio, Napoli (NA), Italy*

Abstract

The present paper describes the design and testing activities carried out on a 1000 N hybrid rocket demonstrator, including a preliminary data assessment. Gaseous oxygen and a paraffin-based solid fuel represent the hybrid propellants. The demonstrator configuration and the design logic are presented first. Later, the experimental results of the test campaign are reported. Results include numerous acquisitions, such as chamber pressure, temperatures and thrust. A preliminary assessment of the experimental data is finally discussed. The demonstrator provided a stable combustion in all the testing conditions and performances in line with the expectations. Throttling capability of the test article was also demonstrated.

1. Introduction

The potential advantages of hybrid rocket engines for space applications, with respect to other rocket typology, have been highlighted over the years by different works in relevant literature (e.g. [1], [2]). As an example, the reduced environmental impact, associated with the use of typical hybrid propellants, makes this technology interesting for replacing the classical systems based on hydrazine. In this specific case, the hybrid technology would guarantee all the requirements together with high performances. Of course, there are other numerous potential advantages associated with the use of hybrid propellants. Nevertheless, the hybrid engine development still requires further effort to reach the same level of maturity as solid and liquid traditional systems. Over the years, some drawbacks have been overcome, such as the low fuel regression rate. Detailed studies presented by Karabeyoglu [2] showed the strong increase in the regression rate with liquefying fuels. This class of polymers allows for a significant increase in the regression rate, with respect to classical ones. Appropriate blending also provide the mechanical characteristics required by typical space applications.

In the present research a selected paraffin-based fuel blend was investigated. The formulation adopted showed very good performances and mechanical properties, when previously tested at subscale level on a 200 N breadboard [3]. Therefore, the same formulation was adopted for scaling-up the propellant grain and moving towards the 1000 N thrust class engine, with a new breadboard design.

An experimental test campaign was carried out on the 1000 N test article, allowing for the investigation of the paraffin-based fuel blend behaviour on a larger scale and wider range of operating conditions. In particular, with respect to subscale experiments, the oxidizer to fuel mixture ratio range was extended. The test article was opportunely equipped to acquire different experimental data. Besides chamber pressure and thrust, temperature of the flow in the pre-chamber and temperature inside the graphite nozzle material were acquired. The latter parameter allows the estimation of the convective heat transfer coefficient in the nozzle region, which is strictly linked to the graphite nozzle thermo-chemical erosion. This is an extremely important parameter to be evaluated, since the throat area enlargement directly affects the motor performances.

The results of the experimental test campaign show that hybrid rocket engine can operate, with good efficiency and stability, in a wide range of operating conditions, confirming some of the advantages over both solid and liquid technologies often mentioned in the relevant literature [1], [4].

DOI: 10.13009/EUCASS2019-541

2. Experimental set-up

2.1 Demonstrator description

A cross section of the demonstrator is shown in Figure 1 with highlighted the sensors adopted for the experimental acquisitions. The injection system is based on a showerhead architecture. It is characterized by seven injector of constant diameter, which ensure a quasi-uniform axial flow at grain port inlet. The injector system is designed such that it can be easily replaced for testing other injector configurations. The external shell of the breadboard is made of stainless steel, and contains the pre-chamber, the propellant grain, post combustion chamber and nozzle. The pre-chamber has a thermal protection system based on graphite and hosts a pressure transducer. Both nozzle and pre-combustion chamber are protected by graphite; the post combustion chamber hosts a further pressure transducer. An embedded thermo-couple is located in proximity of the nozzle throat in order to monitor temperature of the zone. The ignition of the breadboard is assured by a spark plug located in the pre-chamber that ignites a mixture of oxygen and methane injected in the pre-chamber. The propellant grain is a blended paraffin wax including a high percentage of microcrystalline paraffin commercialized by SASOL®, labelled with the trade code 0907. A small amount of a blackening additive was added to the melted wax, which effect is to increase the thermal radiation absorption at the fuel surface improving the regression rate [2], [9].

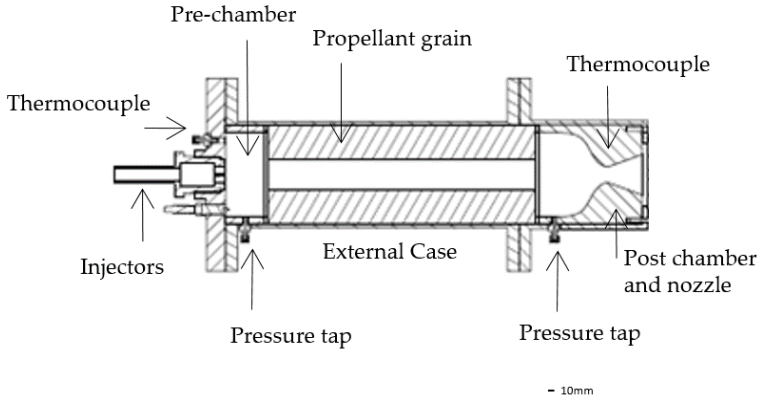

Figure 1: Demonstrator cross section and telemetry

The 1000 N demonstrator completely assembled and ready for the leakage test is shown in Figure 2 on the right. On the left, a picture of the propellant grain before the firing test.

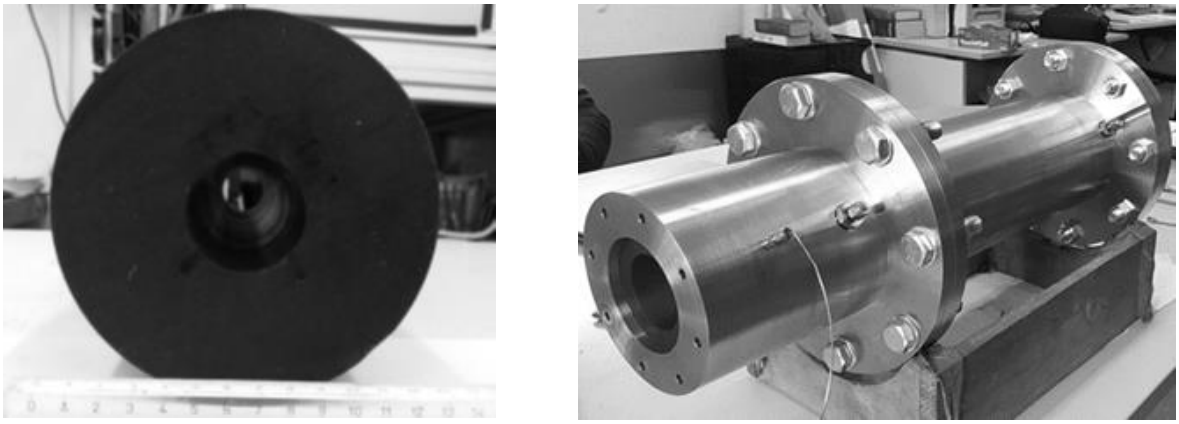

Figure 2: Propellant grain before test (left) and 1000 N demonstrator assembled (right)

2.2 Test rig description and test plan

The test facility is a versatile experimental setup primarily designed for firing hybrid rocket engines of several sizes [3].
The piping and instrumentation schematic of the test rig is shown in Figure 3. Gaseous oxygen is supplied by a reservoir consisting of four cylinders, while pressure regulators set the operating pressure along the breadboard feed line. Oxygen

DOI: 10.13009/EUCASS2019-541

mass flow rate is evaluated through gas temperature and pressure measurements upstream of the throat of a chocked Venturi tube. The Venturi can be dismounted and replaced depending on the requested oxidizer mass-flow rate. For testing the 1000 N breadboard a 5 mm throat orifice was adopted in order to guarantee the flow rate requested.
Nitrogen is purged into the chamber for the burn out and in case of an emergency shutdown.

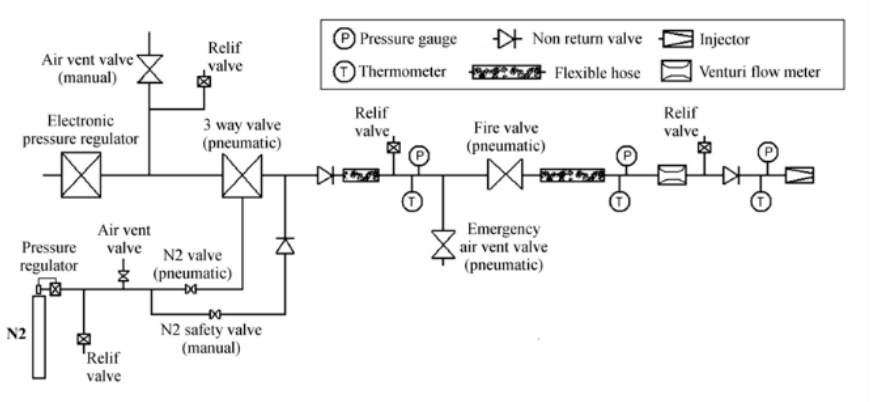

Figure 3: Test rig layout

Firing tests have been conducted with an incremental logic, being the hardware a new design, in order evaluate the behaviour of the test article from lower pressure/duration to higher ones.
The operating conditions of each test are reported in Table 1.

Table 1: Nominal operating conditions

	Test L1	**Test L2**	**Test L3**	**Test L4**	**Test L5**
Oxidizer mass-flow rate (kg/s)	0.120	0.200	0.200	0.140-0.225	0.250
Firing time (s)	6	8	12	5+1 (transient)+4	10

According to the incremental logic, the first test L1 was conducted with about the 50% oxidizer mass-flow rate for a shorter time (6 s) with respect to nominal one. In the second L2 test both oxidizer mass-flow rate and time were increased. In the L3 test the nominal firing time was further increased. Firing test L4 was made to demonstrate throttling capabilities of the breadboard. Test L5 was finally performed with the nominal oxidizer mass-flow rate.
Figure 4 shows the 1000 N breadboard integrated on the test bench. A leakage test was performed before the firing test, using pressurized nitrogen at 0.8 MPa for five minutes, in order to verify the absence of any leaks from internal interfaces.

Figure 4: 1000 N breadboard integrated on the test bench

DOI: 10.13009/EUCASS2019-541

3. Test campaign and data assessment

3.1 Testing activities and acquisitions

All the performed firing tests were successful, no damage in any parts of the test article was observed. The experimental oxidizer mass-flow rates were in line with the test plan; specifically, errors between nominal and experimental measured values were below 10% for all the firing tests. Figure 5-a shows the breadboard during firing test L3, while Figure 5-b shows the propellant grain status at the end of test L3. A quite uniform consumption was observed.

(a) (b)

Figure 5: Rocket plume during firing test L3 (a) and propellant grain after the same firing (b)

Figure 6 provides the temporal evolution of chamber pressure (a) and thrust (b) acquired for the different firing tests. Chamber pressure slightly increases and tends to a constant value during firing time; a similar behaviour is also found in the thrust curves. The throttling test L4 showed a stable behaviour, both thrust and pressure levels were steady for both the operating conditions and the transition appeared stable without spikes and oscillations.
Due to higher regression rates, even if on one side the chamber temperature decreases in time due to decrease of MR from the optimum, the higher paraffin mass-flow rate compensates the result of this effect on chamber pressure. Moreover, chamber pressure was not affected by throat diameter increase, since no ablation was noticed after the firing tests.

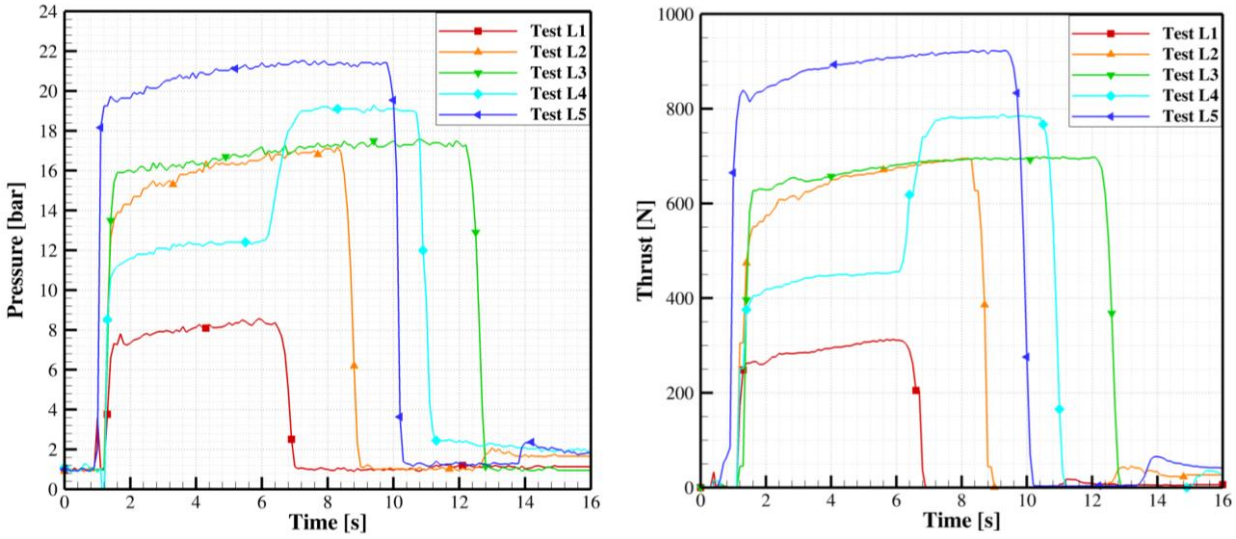

(a) (b)

Figure 6: Measured pressure in the post-chamber (a) and thrust (b) over firing time

Figure 7 shows temperature acquisitions by the thermocouple located in the breadboard pre-chamber (a) and the embedded thermocouple in proximity of the nozzle throat (b). For test L3, the pre-chamber TC did not acquire due to a paraffin occlusion of the hole. In all the cases, the pre-chamber TC revealed a temperature increase at ignition up to a maximum value, then a gradual decrease – more evident for L2 test – up to a significant slope change due to switch-off. The pre-chamber high temperature values are mainly due to hot recirculating gas coming from the grain combustion (see [11] for fluid-dynamics description). Another significant slope change is due to nitrogen purging. It can be observed that highest temperature values are not associated with Test L5, which is the one with highest oxidizer mass-flow rate. It can be also observed that the temperature initially measured in Test L4 is lower than the measured in Test L1, where the oxidizer mass-flow rate is lower. These behaviours are explained observing that for firing test L4 and L5 an anomalous higher fuel-grain consumption occurred in proximity of the grain inlet port, probably associated with the ignition procedure. This overheating leads to slightly lower mixture ratio values than those associated with Test L1 and L2.

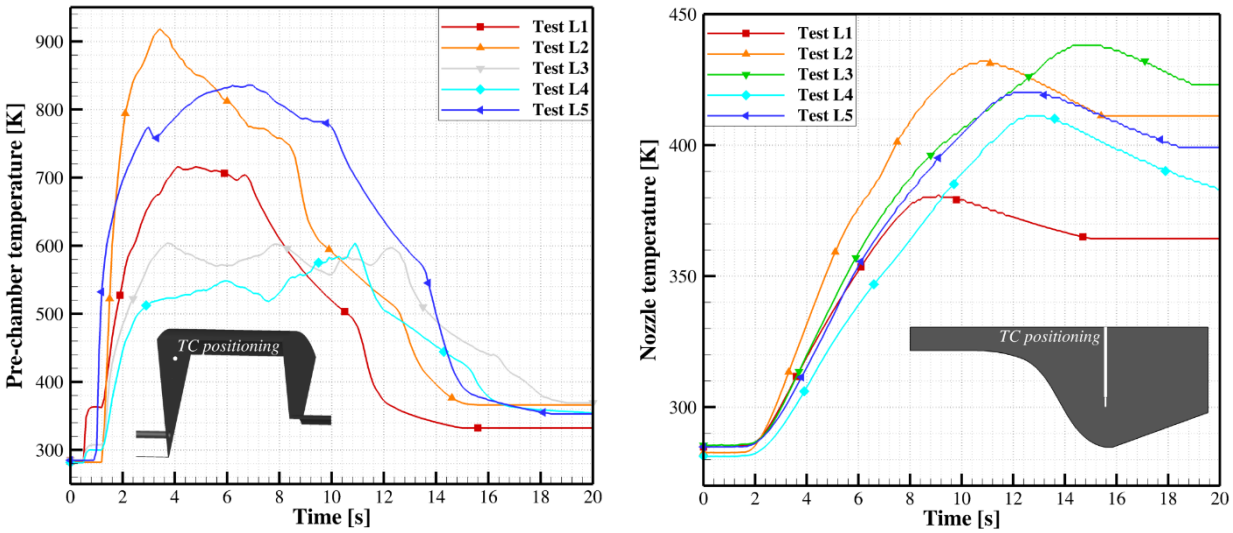

(a) (b)

Figure 7: Measured pre-chamber temperature (a) and nozzle temperature (b) over firing time

Table 2 reports the experimental data acquisitions and measurements for all the firing tests. The time-space averaged fuel regression rate is computed by the fuel mass-loss (which allows the computation of the space-averaged final port diameter). For details on the data reduction technique see [3].

Table 2: Experimental data acquisitions

	Test L1	**Test L2**	**Test L3**	**Test L4**	**Test L5**
Effective firing time (s)	5.6	7.5	11.4	9.7 (5.3+4.4)	9.0
Effective oxidizer mass-flow rate (kg/s)	0.110	0.195	0.192	0.142 – 0.215	0.243
Time-averaged fuel mass-flow rate (kg/s)	0.984	0.152	0.172	0.177	0.204
Time-averaged mixture ratio (-)	1.12	1.29	1.11	-	1.20
Time-space-averaged ox mass-flux (kg/m2s)	55.35	72.35	52.37	53.3	69.94
Time-space averaged fuel regression rate (mm/s)	1.91	2.53	2.49	2.6	2.99

DOI: 10.13009/EUCASS2019-541

Table 3 reports the time-averaged values of pressure, thrust and specific impulse, for all the firing tests. Considering the nominal firing test L5, the time-averaged thrust value is about 900 N (with peak about 930 N) against the design value of 1000 N. This value is in line with the predictions, since the effective oxidizer mass-flow rate was 0.243 kg/s, against the nominal value of 0.260 kg/s. The time-averaged specific impulse for test L5 is 204 s, which is in line with the expected I_{sp} for the considered average mixture ratio; this value can be further improved going up with the oxygen mass flow rate.

Table 3: Experimental 1000 N breadboard performances

	Test L1	**Test L2**	**Test L3**	**Test L4**	**Test L5**
Time-averaged chamber pressure (MPa)	0.79	1.59	1.67	1.23 – 1.90	2.09
Time-averaged thrust (N)	291	650	679	446 – 782	893
Time-averaged specific impulse (s)	142	191	190	173	204

3.2 Fuel grain regression rate

In Figure 8 the time-space averaged fuel regression rate experimental values against the time-space averaged oxidizer mass-flux are reported. As a first consideration, it can be observed that regression rate does not depend only on the oxidizer mass-flux, since tests characterized by similar oxidizer mass-flux exhibited different regression rate values. In particular, test L1 showed a sensibly lower regression rate value, but it was performed with the lowest oxidizer mass-flow rate and the oxidizer to fuel mixture ratio was very low.

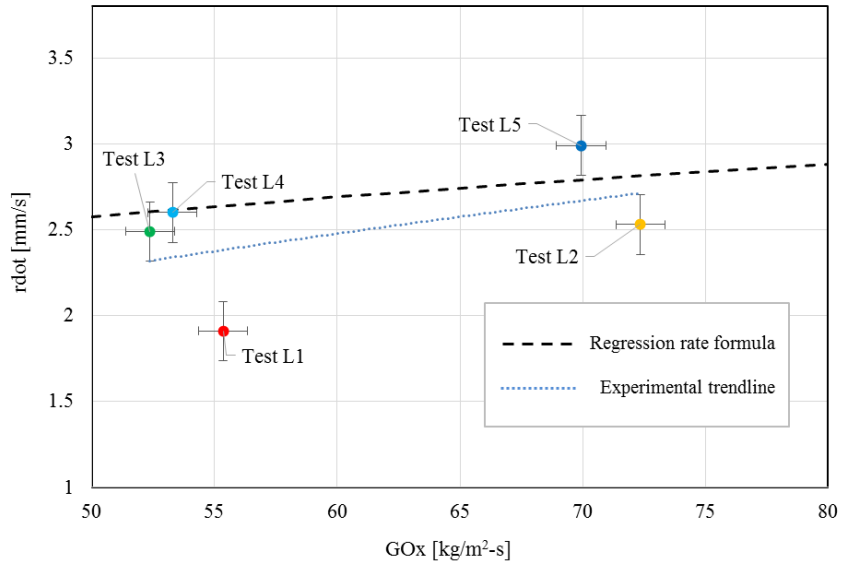

Figure 8: Fuel regression rate against oxidizer mass-flux

Among different factors that could influence the fuel regression rate, the authors consider that the oxidizer to fuel mixture ratio has a strong influence, since it extremely affects the chamber temperature. In particular the test performed are in the MR range between 1 and 2 where slight MR variation leads to important temperature variations. Of course the chamber temperature influences both the vaporization and the entrainment contributions to regression rate, leading to variation of both gas properties and radiative to convective heat-transfer ratio. In particular, higher regression rate values are expected, for the paraffin-based blend under analysis, when the temperature increases.
An experimental evidence of the mixture ratio influence can be found also in Figure 7-a, which shows temperature acquisitions by the thermocouple located in the breadboard pre-chamber. In particular, the gradual temperature decrease after the initial peak value – more evident for L2 test – confirms that mixture ratio decreases over time with respect to the optimum value. As already previously stated, for firing test L4 and L5 an anomalous higher fuel-grain

consumption occurred in proximity of the grain inlet port, leading to slightly lower mixture ratio values in the pre-chamber than those associated with Test L1 and L2.
In order to perform experimental data assessment of the test campaign, a new equation for regression rate, different from the one reported in [3], that could better reproduce the behaviour of the test article for the test condition considered, has been derived. Specifically, the equation was derived by minimizing the differences between the measured fuel mass-loss and those computed by the code (both values are reported in Table 4).

$$\dot{r} = 1.007 * G_{ox}^{0.24} \quad \textbf{(1)}$$

Where $\dot{r}$ is expressed in mm/s while G_{ox} is in $kg/m^2 - s$.
Even if based on few experimental data, the derived regression rate fits well on the experimental values (see Figure 8), except for the test L1 (where the equation reported in [3] remains still valid) for the reason previously explained. It has to be underlined that the regression rate equation can be used for this preliminary assessment activities but a rigorous investigation, based on a significant number of tests, is necessary in order to take into account all the effect influencing regression rate (i.e. mixture ratio, port diameter, chamber pressure).

Table 4: Experimental and numerical fuel mass loss

Test ID	Experimental fuel mass loss (kg)	Numerical fuel mass loss (kg)	Rel. Error %
L2	1.138	1.296	13
L3	1.964	2.111	7
L4	1.743	1.702	3
L5	1.823	1.705	6

3.3 Nozzle wall heat-transfer

The embedded thermo-couple installed in the nozzle allowed the acquisition of temperatures over time for all the firing tests. Results are reported in Figure 7-b. Considering the numerical result given by thermal analysis in nominal testing conditions (Test L5), a strong difference was immediately pointed out. In particular, experimental acquisitions showed lower temperature values with respect to those expected.
Some investigations have been carried out and will be discussed hereinafter.

Numerical estimation of the convective heat-transfer coefficient

The convective heat transfer coefficient is defined by the following formulation.

$$h_g = \frac{\dot{Q}_c}{(T_{wa} - T_{wh})} \quad \textbf{(2)}$$

Where $\dot{q_c}$ represents the convective heat transfer rate per unit area (i.e. the surface heat flux), h_g the hot-gas heat transfer coefficient, T_{wh} the hot-side wall temperature and T_{wa} the adiabatic wall temperature.
Referring to the Test L5, a CFD solution is reported in Figure 9 focusing the attention in the nozzle part of the breadboard, showing temperature contours over the middle plane slice and wall heat-flux over the nozzle surface. Details about CFD setup can be found in [11]. Different results are reported, the convective heat-transfer coefficient value at the nozzle throat is about 5500 W/m-K (highlighted in red).

DOI: 10.13009/EUCASS2019-541

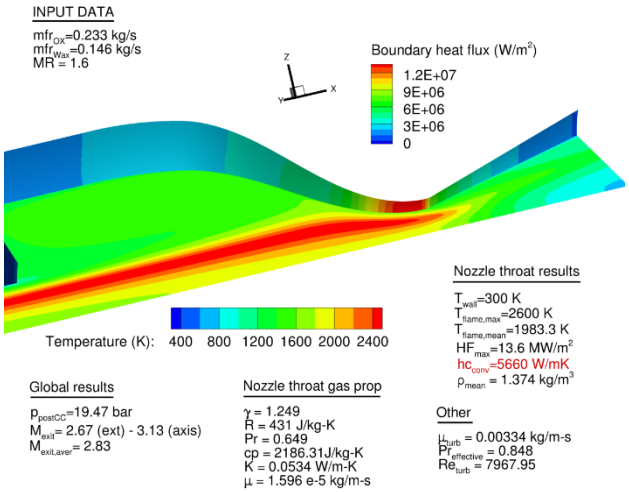

Figure 9: CFD solution for Test L5

Considering the empirical correlation suggested by Ciniaref and Dorovoliski [12], as reported in Eq. 3, the h_g value in nominal firing test conditions was expected to be 4750 W/m-K, as shown in Table 5.

$$h_g = 0.0162\left(\frac{k_{hot}}{2R_c}\right)(Pr^{0.82})(Re^{0.82}) \quad \textbf{(3)}$$

Table 5: h_g values computed by CFD simulation and empirical correlation for Test L5

Test ID	h_g CFD [W/m-K]	h_g empirical [W/m-K]
L5	5660	4750

Even if values given by CFD and empirical correlation differ of about 20 %, the order of magnitude is however similar. The CFD value was adopted for thermo-mechanical analysis, being the most conservative. Under this condition, also erosion of the graphite nozzle throat was expected due to ablation phenomena.

Rebuilding of convective heat-transfer coefficient values

Starting from experimental temperature measurements in the nozzle material, a procedure was adopted to extract the convective heat-transfer coefficient values at the hot-gas side nozzle wall. The experimental value has been obtained by means of numerical transient thermal simulation. Specifically, a first attempt convective heat flux coefficient along the nozzle wall is given as input together with the adiabatic flame temperature value. These two variables are updated each 0.1 seconds and the numerical result, in terms of temperature in the thermo-couple location, is compared with the experimental acquisition. The procedure is repeated until similar values are returned. Properties of the graphite material are specified in Table 6. At the same time, also the nozzle wall temperature is found.

Table 6. Properties of graphite at 300 K

Density [kg/m3]	Th. Conductivity [W/m-K]	Specific Heat [J/kg-K]
1888	133	726

A result is reported in Figure 10 considering the firing test L2. In this case the numerical data reproduces the acquisition with high fidelity in the first three seconds and then it moves away underestimating the experimental measure. In the secondary frame of Figure 10 also the temperature contour plot in the computing domain is shown, including the temperature profile along the nozzle wall at final time.

DOI: 10.13009/EUCASS2019-541

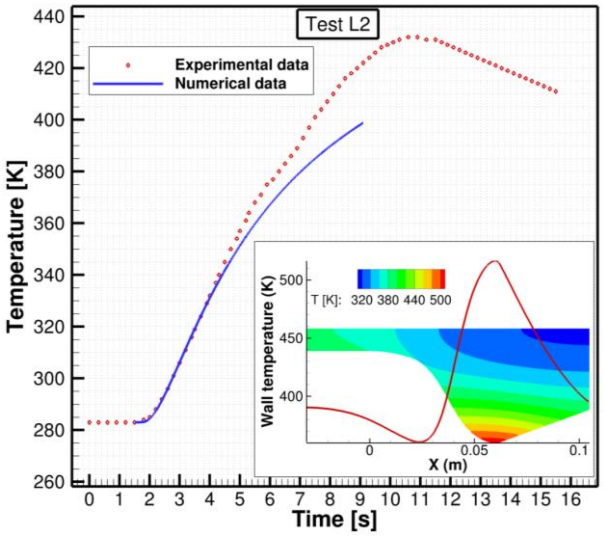

Figure 10: Experimental temperature data and numerical rebuilding against time for firing test L2

Results, in terms of convective heat-transfer coefficient applied at initial time, for all the firing tests (except for Test L4 where the throttling condition would be more difficult to implement) is reported in Figure 11-a.

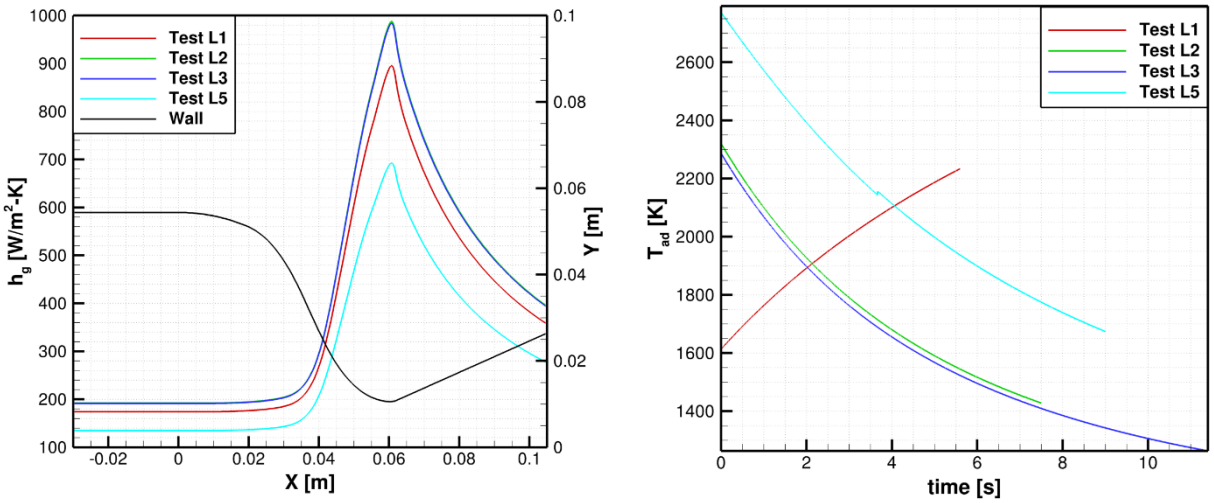

(a) (b)

Figure 11: Convective heat-transfer coefficient values at initial time (a) and adiabatic flame temperature versus time (b) for all the firing tests

As you can see, rebuilding of the experimental acquisition indicates that the measured convective heat transfer coefficient value is below 1000 W/m-K for all the firing tests, including Test L5. It should be pointed out that, even if the h_g value for Test L5 is the lowest one, the T_{ad} value is very high with respect to the others (as visible in Figure 11-b) due to higher oxidizer mass-flow rate and, consequently, mixture ratio. The adiabatic flame temperature data for Test L1 presents an opposite trend since it was derived by applying the regression rate law reported in [3], which is more appropriate with respect to Eq. 1, as stated in section 3.2.

It is also worth noticing that the order of magnitude of the rebuilt h_g is more or less right. This can be asserted looking at Figure 12, where temperatures in the TC location are compared when different h_g numerical values are imposed in the thermal calculation. As you can see, if the h_g applied value strongly differs from the right order of magnitude, the numerical temperature coming out is very different from the acquisition.

DOI: 10.13009/EUCASS2019-541

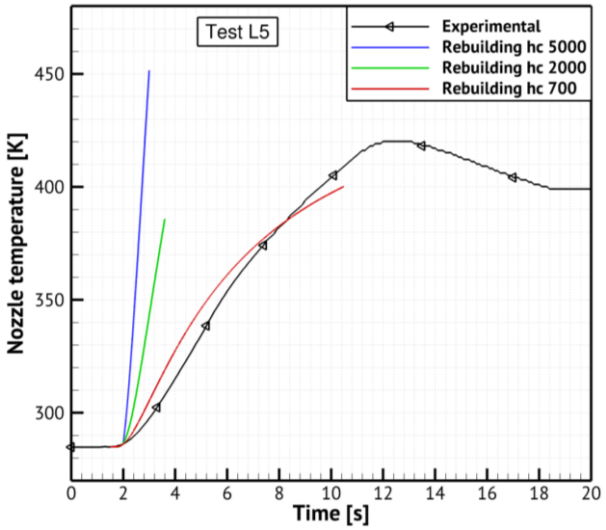

Figure 12: Temperature results with the application of different h_g values

Due to the reduced convective heat transfer coefficient, ablation in the nozzle did not occur, in fact no throat erosion was observed. Moreover, numerical investigation from literature in similar condition provided significant erosion rate of the nozzle throat [13].
This issue requires a particular focus, since it is experimentally found in literature that hybrid rockets based on polymers like HDPE or HTPB show significant erosion rate in similar operating conditions. Of course the importance to account for the erosion rate is well known, since the continuous enlargement of the nozzle throat during the firing directly affects the motor thrust and specific impulse.

5. Conclusion

The design and testing activities of a novel 1000 N HRE breadboard have been presented. The test article, fed with gaseous oxygen and a paraffin-based fuel, showed a robust design and good performances. In particular, a stable combustion occurred in all the testing conditions including a wide range of pressure and mixture ratio. Chamber pressure oscillations were characterized by very low amplitude, analysing high-frequency signals. The breadboard was tested also in order to verify throttling capabilities, oxidizer mass-flow rate was increased of about 35 % during one of the firing test, leading to thrust increase of about 40%. Numerous experimental data were collected, including temperature of the flow in the pre-combustion chamber and temperature inside the nozzle material. The experimental input variables – e.g. oxidizer mass-flow rates – were in agreement with the test plan; the breadboard performances were in line with the predictions. A higher fuel regression rate was experimentally found with respect to subscale results, due to different operating conditions which affected both the gas properties and the heat transfer to the fuel surface. At the end of the campaign, the graphite nozzle throat showed no significant erosion, in contrast with the expectations associated with the pre-testing numerical predictions and literature investigations. The result was due to lower than expected wall temperatures and, therefore heat transfer rate.
Further investigations are still required for a thorough assessment of the collected data. Other test campaigns will be necessary, in order to better assess the role of the mixture ratio on the fuel regression rate.

References

[1] Altman, D., and Holzman, A. Overview and History of Hybrid Rocket Propulsion. Fundamentals of Hybrid Rocket Combustion and Propulsion, edited by K. Kuo, M. Chiaverini, Vol. 218, Progress in Astronautics and Aeronautics, AIAA, 2007, pp. 1–36.
[2] Karabeyoglu, M. A., Cantwell, B. J., Altman, D. Development and Testing Of Paraffin-Based Hybrid Rocket Fuels. AIAA 2001-4503. 37th AIAA/ASME/SAE7ASEE Joint Propulsion Conference and Exhibit. July 8-11, 2001, Salt Lake City, Utah.

[3] Di Martino, G. D., Mungiguerra, S., Carmicino, C., Savino, R., Cardillo, D., Battista, F., Invigorito, M., Elia, G. Two-Hundred-Newton Laboratory-Scale Hybrid Rocket Testing for Paraffin Fuel-Performance Characterization. Journal of Propulsion and Power. doi: 10.2514/1.B37017.
[4] Karabeyoglu, A. Advanced Hybrid Rockets for Future Space Launch. Fifth European Conference for Aeronautics and Space Sciences. 1-5 July 2013. Munich, Germany.
[5] A. Ponomarenko, RPA – Tool for Rocket Propulsion Analysis, Space propulsion conference 2014, Cologne, Germany, SP2014_2967435.
[6] P.G. Hill and C.R. Peterson, Mechanics and thermodynamics of propulsion, Addison-Wesley Pub. Co., 1965
[7] David W. Netzer et al, Hybrid Rocket Internal Ballistics, AD-754 769, 1972.
[8] Vigor Yang et al., Liquid rocket thrust chambers: aspects of modeling, analysis, and design, AIAA v.200, ISBN 1563472236, 2004.
[9] Kumar, C. P., and Kumar, A. A Numerical Study on the Regression Rate of Hybrid Rocket Motors Using a Combination of Enhancement Techniques. AIAA Paper 2012-4105, 2012. doi: 10.2514/6.2012-4105.
[10] Marxman, G. A., Wooldridge, C. E., Muzzy, R. J. Fundamentals of Hybrid Boundary Layer Combustion. Progress in Astronautics and Aeronautics. Vol. 15, 1964 p. 485.
[11] Cardillo, D., Battista, F., Elia, G., Di Martino, G. D., Mungiguerra, S., Savino, R. "Design And Testing Of A Paraffin-Based Hybrid Rocket Demonstrator. Space Propulsion Conference 2018. 14-18 May 2018. Seville, Spain.
[12] Ciniaref, G., D., Dorovoliski , M., B., "Theory of Liquid-Propellant Rockets", Moscow, 1957.
[13] Bianchi, D., Nasuti, F. Numerical Analyses of Nozzle Material Thermochemical Erosion in Hybrid Rocket Engines. Journal of Propulsion and Power. Vol. 29, No. 3, May-June 2013.

Nomenclature

G	port average mass flux [kg/m2-s]
h_g	convective heat transfer coefficient [W/m-K]
p_c	chamber pressure [Pa]
$\dot{Q}_c$	convective heat flux [W/m2]
$\dot{Q}_r$	radiative heat flux [W/m2]
$\dot{r}$	surface regression rate [mm/s]
T	temperature [K]
T_{wa}	adiabatic wall temperature [K]
T_{wh}	hot gas wall temperature [K]
T_{ad}	Adiabatic flame temperature [K]

Greek Symbols

η	combustion efficiency [-]
μ	gas molecular viscosity [kg/m-s]
ρ	density [kg/m^3]
σ	surface tension [N/m]

Subscripts

cc	combustion chamber
g	gas
id	ideal
l	liquid
ox	oxygen
r	real
s	solid

Acronyms

CFD	Computational Fluid Dynamics
HDC	CIRA code
$HDPE$	High Density Polyethylene
HRE	Hybrid Rocket Engine
$HTPB$	Hydroxyl Terminated Polybutadiene
MR	Oxidizer to fuel Mixture Ratio
TRL	Technology Readiness Level